

# Real-Time Interrogation of a Linearly Chirped Fiber Bragg Grating Sensor Based on Chirped Pulse Compression With Improved Resolution and Signal-to-Noise Ratio

Weilin Liu, *Student Member, IEEE*, Ming Li, *Member, IEEE*, Chao Wang, *Student Member, IEEE, OSA*, and Jianping Yao, *Senior Member, IEEE, Fellow, OSA*

**Abstract**—A novel approach to interrogating in real time a linearly chirped fiber Bragg grating (LCFBG) sensor based on spectral-shaping and wavelength-to-time (SS-WTT) mapping with improved interrogation resolution and signal-to-noise (SNR) ratio is proposed and experimentally demonstrated. The proposed system consists of a mode-locked laser source, an optical interferometer incorporating an LCFBG, and a dispersive element. The optical interferometer has a spectral response with an increasing free spectral range (FSR). The incorporation of the LCFBG in the interferometer would encode the sensing information in the spectral response as a change in the FSR. After SS-WTT mapping, a linearly chirped microwave waveform is obtained. The correlation of the linearly chirped microwave waveform with a chirped reference waveform would provide a sharp correlation peak with its position indicating the wavelength shift of the LCFBG. A theoretical analysis is carried out, which is validated by a numerical simulation and an experiment. The experimental results show that the proposed system can provide an interrogation resolution as high as  $0.25 \mu\text{m}$  at a speed of 48.6 MHz.

**Index Terms**—Chirped microwave pulse, cross-correlation, dispersion, dispersive Fourier transformation, fiber Bragg grating (FBG), wavelength-to-time mapping.

## I. INTRODUCTION

**F**IBER BRAGG grating (FBG) sensors have been investigated extensively in the last few decades which could find numerous applications such as structural health monitoring, molecular dynamics sensing and aircraft engine diagnostics. Compared with conventional electro-mechanical sensors, FBG sensors possess unique advantages, such as immunity to electromagnetic interference (EMI), high resistance to chemical corrosion, light weight, and ease in signal transmission. Most of the FBG sensors are interrogated by monitoring the wavelength shift. Technically, the wavelength-encoded characteristic of an

FBG sensor presents high robustness to noise and power fluctuations, which also makes wavelength division multiplexing (WDM) [1], [2] in FBG sensor array systems achievable. Based on these essential attributes, numerous demodulation or interrogation techniques have been proposed and demonstrated in the last few years.

For an FBG sensor that is interrogated by monitoring the wavelength shift, an optical spectrum analyzer (OSA) is usually used. The use of an OSA could provide high measurement accuracy, but the measurement speed is low. To increase the measurement speed, various techniques have been proposed. These techniques can be implemented based on passive detection [3]–[9] or active detection [10]–[12]. Passive detection is usually realized based on optical power monitoring using an optical edge filter [3], [4], a Fabry-Pérot filter [5], or a charge coupled device (CCD) spectrometer [7], [8]. Technically, the edge filter functions as a static frequency discriminator to convert the wavelength shift into intensity change or intensity spatial displacement. The advantage of passive detection is that the system is simple and less costly, but the power variations from the light source would be reflected as the detector output, making the interrogation have poor accuracy. The use of active detection could eliminate the impact of power fluctuations on the measurement accuracy. In general, an active detection scheme is implemented based on an interferometric scanner and the wavelengths shift in the FBG sensor is usually reflected as a change in an optical phase. Therefore, the measurement resolution is much improved compared with the passive detection schemes. In active detection schemes, the interference structure could be an unbalanced Mach-Zehnder interferometer (MZI) [10], a Michelson interferometer [11], or a long-period fiber grating (LPG) pair interferometer [12]. However, an active scheme based on an optical interferometer is sensitive to environmental changes, such as temperature change, subtle vibrations, or even air fluctuations, which would deteriorate significantly the system stability. In addition, a piezoelectric transducer (PZT) is usually employed as the scanning device [10]. The speed of a PZT is in the range of kilo Hertz. For applications where an ultra-fast interrogation is needed, the active schemes may not fulfill the task.

To improve the interrogation speed, we have recently proposed and experimentally demonstrated a technique to measure the wavelength shift in the temporal domain based on spectral-shaping and wavelength-to-time (SS-WTT) mapping

Manuscript received December 30, 2010; revised February 14, 2011; accepted February 27, 2011. Date of publication March 07, 2011; date of current version April 08, 2011. This work was supported by the Natural Science and Engineering Research Council of Canada (NSERC).

The authors are with the Microwave Photonics Research Laboratory, School of Information Technology and Engineering, University of Ottawa, ON K1N 6N5, Canada (e-mail: jpyao@site.uottawa.ca).

Color versions of one or more of the figures in this paper are available online at <http://ieeexplore.ieee.org>.

Digital Object Identifier 10.1109/JLT.2011.2123081

using an ultra-short pulsed source and a dispersive element [13]. It is known that a pulsed source through a dispersive element would experience pulse broadening. If the pulse is ultra-short, the output from the dispersive element would be a Fourier transformed version of the input pulse [14], [15]. The operation is called real-time Fourier transformation or wavelength-to-time (WTT) mapping [16], [17]. Following this concept, we demonstrated an interrogation system at a high speed. In the system, the spectrum of an ultra-short pulse is shaped by an FBG or FBG array, and the shaped-spectrum is then mapped to the time domain in a dispersive element. The measurement is then done in the time domain using a high speed oscilloscope. The major limitation of using a FBG or FBG array in this technique is that the spectrum of a FBG is narrow; after WTT mapping, the temporal pulse has a low power level, leading to poor signal-to-noise ratio (SNR). The use of an FBG with a wider spectrum would increase the SNR, but the interrogation resolution would be poorer. Therefore, there is a tradeoff between the SNR and the resolution [13].

In this paper, we propose a novel technique to interrogate an FBG sensor based on SS-WTT mapping using a linearly chirped FBG (LCFBG), with both improved SNR and resolution. The LCFBG is incorporated in one arm of a Mach-Zehnder interferometer (MZI). Due to the wavelength dependent nature of the length of the arm with the incorporated LCFBG, the MZI would have a spectral response with increasing free spectral range (FSR). An optical pulse from a mode-locked laser source is spectrally shaped by the MZI and its spectrum is then mapped to the temporal domain by the dispersive element. Due to the linear WTT mapping, a chirped microwave waveform with a shape that is a scaled version of the shaped spectrum is generated. The chirped waveform is detected by a photodetector (PD) and sent to a digital processor to perform pulse compression.

It is known that a chirped waveform can be compressed [18] if it is sent to a correlator in which a reference that is identical to the chirped pulse is correlated with the chirped waveform [19]. The key significance here is that the wavelength shift is estimated by measuring the location of the correlation peak, with both improved resolution and SNR. The correlation is done here by building a special reference waveform, which is a linearly chirped waveform with a chirp rate identical to that of the generated chirped microwave waveform, but with an instantaneous frequency extending from the smallest to the largest possible values corresponding to the generated chirped microwave waveform when the LCFBG is experiencing the largest and the smallest wavelength shift. Therefore, the location of the correlation peak would indicate the wavelength shift.

The paper is organized as follows. In Section II, the principle of the proposed technique is presented. The expression for the generated chirped microwave waveform is developed and the design of the special reference waveform is provided. The expression for the correlation between the generated chirped microwave waveform and the special reference waveform is also derived. In Section III, a numerical simulation is implemented in which an LCFBG sensor interrogation system with pulse compression to improve the resolution and SNR is performed. In Section IV, an experiment is performed to verify the proposed approach. An interrogation resolution as high as  $0.25 \mu\text{e}$  at a speed of 48.6 MHz is demonstrated.

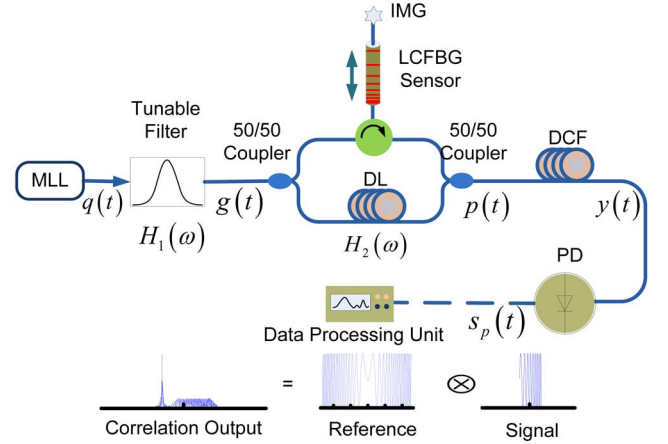


Fig. 1. Schematic of an LCFBG sensor interrogation system based on SS-WTT mapping. MLL: mode-locked laser; LCFBG: linearly chirped fiber Bragg grating; DL: delay line; DCF: dispersion compensating fiber; PD: photodetector.

## II. PRINCIPLE

The proposed interrogation system is shown in Fig. 1. It consists of a mode-locked laser source, a tunable optical filter, an MZI incorporating an LCFBG in one arm of the MZI, a dispersion compensating fiber (DCF) serving as a dispersive element for linear WTT mapping, and a PD. An ultra-short pulse generated by the mode-locked laser is sent to the MZI through a tunable optical filter. The tunable optical filter is employed to control the temporal width of the pulse to the MZI. The spectrum of the pulse from the tunable optical filter is then shaped by the MZI. At the output of the MZI, an optical spectrum with an increasing or decreasing FSR is generated. Note that an offset of the FSR profile would be resulted if the wavelength of the LCFBG is shifted. Thus, the information, such as a strain applied to the LCFBG, is coded in the shaped spectrum. After WTT mapping in the DCF, a linearly chirped microwave waveform is obtained at the output of the PD. The chirped microwave waveform is then sent to a digital processor to perform a correlation with a special reference waveform. The location of the correlation peak would indicate the wavelength shift of the LCFBG. Since the spectrum of the LCFBG is much wider than a uniform FBG, the proposed interrogation system would provide a better SNR, at the same time with a high resolution. In the following, an analysis is provided to show the operation of the proposed technique.

Assume that the tunable optical filter has a transfer function with a Gaussian profile, given by

$$H_1(\omega) = A_1 \exp \left[ -\frac{1}{2} \left( \frac{\omega - \omega_{F0}}{B_F} \right)^2 \right] \quad (1)$$

where  $A_1$ ,  $\omega_{F0}$  and  $B_F$  are the amplitude, the central frequency and the bandwidth of the tunable optical filter, respectively. The pulse at the output of the tunable filter is given by

$$G(\omega) = H_1(\omega)Q(\omega) \approx A_1 \exp \left[ -\frac{1}{2} \left( \frac{\omega - \omega_{F0}}{B_F} \right)^2 \right] \quad (2)$$

where  $Q(\omega)$  and  $G(\omega)$  are the Fourier transforms of  $q(t)$  and  $g(t)$ , respectively. Considering that the input pulse to the tunable optical filter is ultra-short, then we can model, for simplicity, the input pulse as a unit impulse, that is,  $q(t) = \delta(t)$ .

To generate a frequency-chirped pulse, an unbalanced MZI incorporating an LCFBG in one arm is employed. Compared to a conventional MZI with a constant FSR, our MZI has an increasing or decreasing FSR. Mathematically, the unbalanced MZI incorporating an LCFBG in one arm can be modeled as a two-tap delay-line filter with a transfer function given by

$$\begin{aligned} H_2(\omega) &\cong \frac{1}{2} \left[ \exp \left( -j\omega t_1 + j \frac{\ddot{\Phi}_v}{2} \omega^2 \right) + \exp(-j\omega t_2) \right] \\ &= \frac{\sqrt{2}}{2} \sqrt{1 + \cos \left( \frac{\ddot{\Phi}_v}{2} \omega^2 + \omega \Delta t \right)} \\ &\quad \times \exp \left( -j\omega t_1 + j \frac{\ddot{\Phi}_v \omega^2 - \omega \Delta t}{2} \right) \end{aligned} \quad (3)$$

where  $t_1$  and  $t_2$  are the time delays in the two MZI arms,  $\ddot{\Phi}_v = d^2\theta(\omega)/d\omega^2|_{\omega=\omega_0}$  (ps<sup>2</sup>) is the first-order dispersion coefficient of the LCFBG, and  $\Delta t = t_2 - t_1$  is the time delay difference between the two arms of the unbalanced MZI. Since the higher order dispersion is small, only the first-order dispersion of the LCFBG is considered.

For a given wavelength, assume that the length difference between the two arms without a strain applied to the LCFBG is  $\Delta L$ , the additional length difference caused by a strain is then given by  $2\Delta\lambda/C$ , where  $\Delta\lambda$  is the wavelength shift of the LCFBG, which is also a function of the applied strain, and  $C$  (nm/cm) is the chirp parameter of the LCFBG. Thus, the total time difference is given by

$$\Delta t = \left( \Delta L + \frac{2\Delta\lambda}{C} \right) \frac{n_{\text{eff}}}{c} \quad (4)$$

where  $n_{\text{eff}}$  is the effective refractive index of the optical fiber, and  $c$  is the speed of light in vacuum.

The magnitude response of the transfer function (3) could be simplified as  $|\cos(\ddot{\Phi}_v \omega^2/4 + \Delta t \omega/2)|$ , which determines the interference fringe pattern of the MZI. The first-order dispersion  $\ddot{\Phi}_v$  determines the frequency chirp rate, and the time-delay difference  $\Delta t$  consists of two parts: the first part,  $\Delta L n_{\text{eff}}/c$ , is wavelength-independent, which determines an offset central frequency; the second part,  $2\Delta\lambda n_{\text{eff}}/(Cc)$ , is wavelength-dependent, which determines the central frequency shift of the generated chirped pulse due to the sensing information change. Therefore, the MZI accomplishes two functions: spectral shaping for chirped pulse generation and sensing information encoding.

The pulse at the output of the tunable optical filter is then sent to the MZI to perform spectral shaping. At the output of the MZI, we have

$$\begin{aligned} P(\omega) &= H_2(\omega)G(\omega) \\ &= \frac{\sqrt{2}}{4} A_1 \exp \left[ -\frac{1}{2} \left( \frac{\omega - \omega_{F0}}{B_F} \right)^2 \right] \end{aligned}$$

$$\begin{aligned} &\times \sqrt{1 + \cos \left( \frac{\ddot{\Phi}_v}{2} \omega^2 + \omega \Delta t \right)} \\ &\times \exp \left[ -j\omega \left( t_1 + \frac{\Delta t}{2} \right) \right] \exp \left( j \frac{\ddot{\Phi}_v \omega^2}{4} \right) \\ &= P_1(\omega) \exp \left( j \frac{\ddot{\Phi}_v \omega^2}{4} \right) \end{aligned} \quad (5)$$

where

$$\begin{aligned} P_1(\omega) &= \frac{\sqrt{2}}{4} A_1 \exp \left[ -\frac{1}{2} \left( \frac{\omega - \omega_{F0}}{B_F} \right)^2 \right] \\ &\times \sqrt{1 + \cos \left( \frac{\ddot{\Phi}_v}{2} \omega^2 + \omega \Delta t \right)} \\ &\times \exp \left[ -j\omega \left( t_1 + \frac{\Delta t}{2} \right) \right]. \end{aligned} \quad (6)$$

The effect of the first-order dispersion  $\ddot{\Phi}_v$  in (5) is large and cannot be ignored. In the following treatment, considering the system is linear and time-invariant, the dispersion from the LCFBG can be combined with the dispersion of the DCF, to perform jointly the WTT mapping. The total dispersion for the WTT mapping is  $\ddot{\Phi} = \ddot{\Phi}_v/2 + \ddot{\Phi}_D$ , where  $\ddot{\Phi}_D$  is the first-order dispersion of the DCF. The temporal waveform at the output of the DCF is given by [20]

$$y(t) \approx \exp \left( j \frac{1}{2\ddot{\Phi}} t^2 \right) P_1(\omega)|_{\omega=t/\ddot{\Phi}}. \quad (7)$$

By applying the waveform at the output of the DCF to a PD, we have a photocurrent, given by

$$s_p(t) = R|y(t)|^2 \quad (8)$$

where  $R$  is the responsivity of the PD.

For calculation convenience, (7) is rewritten as a function of wavelength. Substituting (7) into (8) yields

$$\begin{aligned} s_p(t) &\cong T(\lambda) \cdot \left\{ 1 + \cos \left[ \frac{2\pi n_{\text{eff}}}{\lambda_0^2} \lambda \left( \frac{1}{C} \lambda + \Delta L + \frac{2}{C} \Delta \lambda \right) \right] \right\} \Big|_{\lambda=t/\ddot{\Phi}_\lambda} \\ &= T \left( \frac{t}{\ddot{\Phi}_\lambda} \right) \left\{ 1 + \cos \left[ \frac{2\pi n_{\text{eff}}}{C \lambda_0^2 \ddot{\Phi}_\lambda^2} t \right. \right. \\ &\quad \left. \left. \times (t + 2\Delta t_c(z) + C \ddot{\Phi}_\lambda \Delta L) \right] \right\} \end{aligned} \quad (9)$$

where  $T(\lambda)$  is a window function determined by the transfer function of the tunable optical filter  $H_1(\omega)$ ,  $\lambda_0$  is the central wavelength corresponding to  $\omega_0$ , and the mapping relation is given  $\lambda = t/\ddot{\Phi}_\lambda$  with  $\ddot{\Phi}_\lambda = -2\pi c \ddot{\Phi}/\lambda^2$  (ps/nm). Based on (9), the instantaneous frequency of the microwave waveform is given

$$f = \frac{1}{2\pi} \frac{d\phi}{dt} = \frac{n_{\text{eff}} |\Delta L|}{\lambda_0^2 \ddot{\Phi}_\lambda} \pm \frac{2n_{\text{eff}}}{C \lambda_0^2 \ddot{\Phi}_\lambda^2} [t + \Delta t_c(z)]. \quad (10)$$

As can be seen from (10) the received signal at the output of the PD is a linearly chirped microwave waveform, and the measurand information is coded in  $\Delta t_c(z)$ . By correlating the linearly chirped microwave waveform with a special reference waveform, a correlation peak will be generated. The location of the peak will give the information of  $\Delta t_c(z)$ , and hence the wavelength shift.

The special reference waveform is a linearly chirped waveform with an instantaneous frequency extending from the smallest to the largest possible frequency corresponding to the generated chirped waveform when the LCFBG is experiencing the largest and the smallest wavelength shift. Therefore, the correlation between the generated chirped waveform with the special reference waveform will generate a sharp correlation peak and the peak location would indicate the wavelength shift. In building the special reference waveform, the instantaneous frequency of the reference waveform should cover the entire frequency range of the received chirped microwave waveform for the LCFBG experiencing the largest and the smallest wavelength shift. Mathematically, the special reference waveform can be expressed as

$$s_r(t) = \text{rect}\left(\frac{t}{T_1}\right) \cos(2\pi f_0 t + \pi k t^2) \quad (11)$$

where  $\text{rect}(t/T_1)$  is a rectangular window and the width of the window is  $T_1$ ,  $f_0 = n_{\text{eff}}|\Delta L|/(\lambda_0^2 \ddot{\Phi}_\lambda)$  is the initial frequency of the chirped pulse, and  $k = 2n_{\text{eff}}/(C\lambda_0^2 \ddot{\Phi}_\lambda^2)$  is the chirp rate. The received linearly chirped microwave waveform in (9) can be simplified to have a similar expression

$$s_p(t) \cong \text{rect}\left(\frac{t}{T_2}\right) \cos[2\pi f_0 t + \pi k \Delta t_c(z) t + \pi k t^2] \quad (12)$$

where  $T_2 (T_2 < T_1)$  is the time duration of the received linearly chirped microwave waveform. Note that the envelope of the generated chirped waveform is Gaussian-shaped. In (12) we use a rectangular envelop to replace the Gaussian envelop, which will simplify the mathematical derivations.

Rewriting (11) and (12), we have

$$s_r(t) = \text{Re} \{s_{T_1}(t) e^{j2\pi f_0 t}\} \quad (13)$$

where  $s_{T_1}(t) = \text{rect}(t/T_1) e^{j\pi k t^2}$  and

$$s_p(t) = \text{Re} \{s_{T_2}(t) e^{j2\pi f_0 t}\} \quad (14)$$

where  $s_{T_2}(t) = \text{rect}(t/T_2) e^{j\pi k [\Delta t_c(z) t + t^2]}$ .

Hence, the correlation between the generated chirped microwave waveform and the special reference is given as

$$R_{12}(\tau) = \text{Re} \{R_{T_1 T_2}(\tau) e^{j2\pi f_0 \tau}\} \quad (15)$$

where  $R_{T_1 T_2}(\tau) = 1/2 s_{T_1}^*(-\tau) * s_{T_2}(\tau)$ , and  $(*)$  denotes the convolution operation. Equation (15) can be further written as

$$R_{12}(\tau) = \frac{1}{2} w(\tau) \text{sinc} \left\{ \pi k \left[ \tau + \frac{\Delta t_c(z)}{2} \right] w(\tau) \right\} \times \cos(2\pi f_e \tau + \varphi) \quad (16)$$

where  $w(\tau)$ ,  $f_e$  and  $\varphi$  are, respectively, given by

$$w(\tau) = \begin{cases} \frac{T_1+T_2}{2} + \tau, & -\frac{T_1+T_2}{2} \leq \tau < -\frac{T_1-T_2}{2} \\ \frac{T_2}{2}, & -\frac{T_1-T_2}{2} \leq \tau < \frac{T_1-T_2}{2} \\ \frac{T_1+T_2}{2} - \tau, & \frac{T_1-T_2}{2} \leq \tau < \frac{T_1+T_2}{2} \\ 0, & \text{otherwise} \end{cases} \quad (17)$$

$$f_e = \begin{cases} f_0 - \frac{k}{2} \left( \frac{T_1-T_2}{2} + \frac{\Delta t_c(z)}{2} \right), & -\frac{T_1+T_2}{2} \leq \tau < -\frac{T_1-T_2}{2} \\ f_0 - \frac{k}{2} \tau, & -\frac{T_1-T_2}{2} \leq \tau < \frac{T_1-T_2}{2} \\ f_0 + \frac{k}{2} \left( \frac{T_1-T_2}{2} - \frac{\Delta t_c(z)}{2} \right), & \frac{T_1-T_2}{2} \leq \tau < \frac{T_1+T_2}{2} \\ 0, & \text{otherwise} \end{cases} \quad (18)$$

and

$$\varphi = \begin{cases} -\frac{1}{4} \pi k (T_1 - T_2) C \ddot{\Phi}_\lambda \Delta t_c(z), & -\frac{T_1+T_2}{2} \leq \tau < -\frac{T_1-T_2}{2} \\ -\frac{1}{4} \pi k (T_1 - T_2) C \ddot{\Phi}_\lambda \Delta t_c(z), & -\frac{T_1-T_2}{2} \leq \tau < \frac{T_1-T_2}{2} \\ 0, & \text{otherwise.} \end{cases} \quad (19)$$

The correlation function in (16) establishes a straightforward mathematical relationship between the peak location and the time difference caused by the wavelength shift of the LCFBG. The correlation function is a Sinc function, and the first zero points are at  $\tau + \Delta t_c(z)/2 = \pm 1/B_r$ , where  $B_r = kT_2$  is the bandwidth of the received microwave signal. If the chirp bandwidth increases the first zero points would shift in a way such that the mainlobe of the correlation function would be narrow and thus increasing the resolution of the LCFBG sensor. For example, to obtain a compression ratio of 100 for a 400 ps pulse, the bandwidth of the microwave pulse should be 5 GHz, which means that the chirp rate of the microwave pulse should be 0.0125 GHz/ps. In addition, the relationship between the applied strain and wavelength shift is given by [21]

$$\Delta \lambda_c = \lambda_0 (1 - \rho_\alpha) \Delta \varepsilon \quad (20)$$

where  $\rho_\alpha$  is the photoelastic coefficient of the LCFBG fiber. This coefficient is determined by the refractive index and the fiber-optic strain tensor. Considering (4), (10), (16), and (20), we have

$$\Delta \varepsilon = -\frac{1}{2\lambda_0 \ddot{\Phi}_\lambda (1 - \rho_\alpha)} \Delta t_c(z). \quad (21)$$

From (21), we can see that the wavelength shift is a linear function of the peak location of the correlation.

### III. NUMERICAL SIMULATION

In the proposed real-time LCFBG sensor interrogation system, the correlation between the linearly chirped microwave waveform and the special reference would demodulate the measurement information in which the wavelength shift is obtained by measuring the location of the correlation peak. Since the correlation peak is narrow due to the pulse compression, the resolution is improved. In addition, it is well known for a waveform that is embedded in a stationary white noise, the correlation between the waveform and its reference would provide a maximum SNR. Therefore, the tradeoff between the resolution and SNR existing in [13] will no longer exist here.

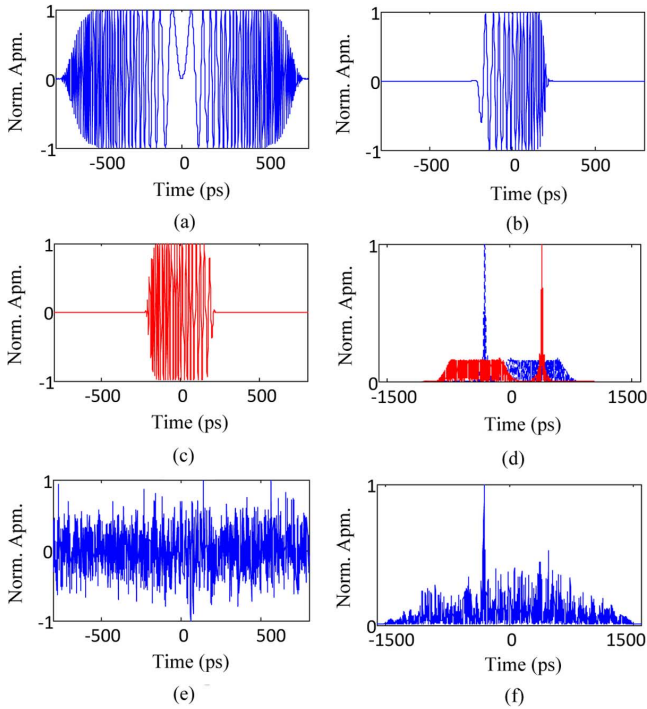


Fig. 2. Simulation results. (a) The reference microwave waveform which has an instantaneous frequency range from 0 GHz to 47.6 GHz. (b) A linearly chirped microwave waveform with  $\Delta t_c = 300$  ps. (c) A linearly chirped microwave waveform with  $\Delta t_c = -300$  ps. (d) The correlation outputs. The red (online version) dashed curve shows the correlation with the waveform shown in (b), and the blue (online version) solid curve shows the correlation with the waveform shown in (c). (e) The waveform in (b) with an added stationary white noise. (f) The correlation with the noisy waveform shown in (e).

In the following, a simulation is performed to demonstrate the operation of the proposed system for the LCFBG sensor interrogation with an improved resolution and SNR.

First, we build a special reference waveform. The special reference waveform is a linearly chirped waveform which is identical to that of the generated chirped microwave waveform, but with an instantaneous frequency extending from the smallest to the largest possible values corresponding to the generated chirped microwave waveform when the LCFBG is experiencing the largest and the smallest wavelength shift. Since the central frequency of the generated chirped waveform can be controlled by tuning the time delay in the lower arm of the MZI, to ease the need for high frequency components, the central frequency of the special reference waveform is accordingly controlled zero. Thus, the special reference waveform has a chirp rate that is  $-0.068$  GHz/ps for  $t < 0$  and  $0.068$  GHz/ps for  $t > 0$ , as shown in Fig. 2(a). The time duration of the special reference waveform is 1400 ps, covering an instantaneous frequency from 47.6 GHz to 0 GHz for  $t < 0$  and 0 GHz to 47.6 GHz for  $t > 0$ .

Then, two linearly chirped microwave waveforms corresponding to two wavelength shifts of 0.185 nm and 0.740 nm are generated. The two waveforms have a super Gaussian envelope with a time duration of 400 ps, as shown in Fig. 2(b) and (c). The first waveform has a chirp rate of 0.068 GHz/ps, and the instantaneous frequency is from 6.8 to 34.0 GHz, corresponding to a wavelength shift of the LCFBG of 0.185 nm. The second waveform has a chirp rate of  $-0.068$  GHz/ps,

and the instantaneous frequency is from 40.8 to 13.6 GHz, corresponding to a wavelength shift of the LCFBG of 0.740 nm.

The two generated linearly chirped microwave waveforms are then correlated with the special reference waveform. The results are shown in Fig. 2(d). As can be seen, two correlation peaks corresponding to the two linearly chirped microwave waveforms are observed. The locations of the two peaks reveal the wavelength shift information. Since the pulse is compressed by 133 times, the resolution is improved by 133 times. To evaluate the robustness of the interrogation system to noise, a stationary white noise is added to the waveform shown in Fig. 2(b), to make the linearly chirped microwave waveform have an SNR of 0 dB. The waveform with an added noise is shown in Fig. 2(e). The correlation of the noisy waveform with the special reference waveform is shown in Fig. 2(f). As expected, a sharp and clear correlation is observed. Based on the correlation output, the wavelength shift can be accurately estimated.

#### IV. EXPERIMENT

An experiment based on the setup shown in Fig. 1 is then implemented. A transform-limited ultra-short Gaussian pulse train at a repetition rate of 48.6 MHz from a passively mode-locked laser source is sent to an optical tunable filter. An individual pulse in the pulse train has a FWHM (full-width at half-maximum) of 394 fs and center wavelength of 1558 nm. The optical tunable filter has a bandwidth of 0.3 nm and the central wavelength is tuned at 1559.59 nm. Then, the spectrally stretched ultra-short pulse is sent to the MZI. An LCFBG is incorporated in the upper arm of the MZI. The LCFBG is 11.5 cm long with a center Bragg wavelength of 1558.7 nm and a value of dispersion of  $-1347$  ps/nm. The lower arm of the MZI has a tunable time delay line. With no strain, the time delay is tuned such that the MZI has a spectral response corresponding to a linearly chirped waveform with a central frequency of zero and a chirp rate of  $-0.068$  GHz/ps for  $t < 0$  and  $0.068$  GHz/ps for  $t > 0$ , as shown in Fig. 3(a).

When a strain is applied, the FSR of the MZI is changed. The spectrally shaped waveform is then sent to a DCF. The total dispersion for WTT mapping is given by  $\ddot{\Phi} = \ddot{\Phi}_v/2 + \ddot{\Phi}_D$ , which is  $2088.1$  ps<sup>2</sup>. A high-speed PD is connected to the output of the DCF. A linearly chirped microwave waveform with its instantaneous frequency indicating the wavelength shift of the LCFBG is generated at the PD, which is sent to a digital signal processor for pulse compression.

Fig. 3(b), (c), and (d) shows three linearly chirped microwave waveforms corresponding to three strains of  $71.5$   $\mu\epsilon$ ,  $406.9$   $\mu\epsilon$ , and  $484.2$   $\mu\epsilon$  applied to the LCFBG, respectively. The correlation of the three linearly chirped microwave waveforms with the special reference waveform given in Fig. 3(a) is shown in Fig. 3(e). The waveforms are highly compressed. The locations of the three peaks indicate the wavelength shifts of the LCFBG are 0.087 nm, 0.495 nm, and 0.589 nm, corresponding to three different strains of  $71.5$   $\mu\epsilon$ ,  $406.9$   $\mu\epsilon$ , and  $484.2$   $\mu\epsilon$ .

Since the highest temporal resolution of the oscilloscope is about 1 ps, and the compression ratio is calculated to be 50.2, the measurement resolution is  $0.25$   $\mu\epsilon$  by (21). Compared with the results reported in [10], where the static resolution was 0.83  $\mu\epsilon$  with a uniform FBG, the approach here clearly demonstrates

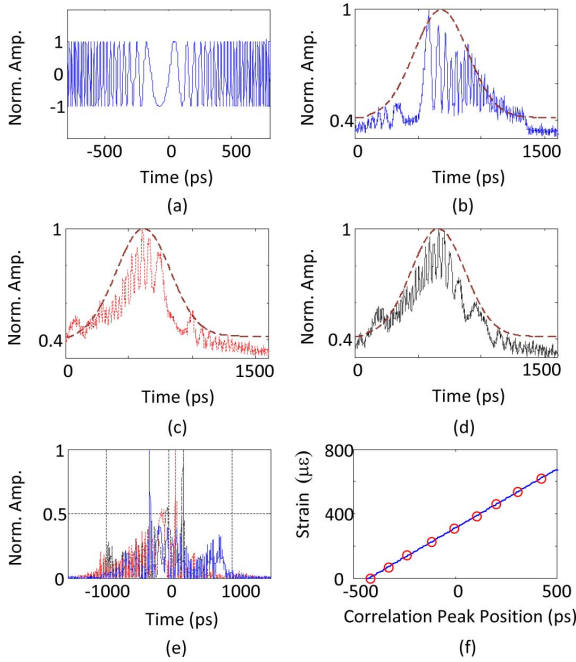


Fig. 3. Experimental results. (a) The special reference waveform. (b) A linearly chirped microwave waveform when a strain of  $71.5 \mu\epsilon$  is applied to the LCFBG. (c) A linearly chirped microwave waveform when a strain of  $406.9 \mu\epsilon$  is applied to the LCFBG. (d) A linearly chirped microwave waveform when a strain of  $484.2 \mu\epsilon$  is applied to the LCFBG. (e) Correlation outputs for the microwave waveforms shown in (b), (c) and (d). (f) Correlation peak position versus the applied strain, the circles are the experimental data, and the solid line shows the linear fitting of the experimental data.

an increased resolution. Fig. 3(f) shows the correlation peak position vs the applied strain. As can be seen the peak position is highly linear with the applied strain, which validates the theoretical conclusion given by (21). The sensitivity of the proposed system is also measured, which is  $1.262 \text{ ps}/\mu\epsilon$ . The responsivity of the LCFBG is measured by an OSA, which is  $1.217 \text{ pm}/\mu\epsilon$ . According to (21), the sensitivity of our proposed system is determined by both the first-order dispersion coefficient  $\ddot{\Phi}_\lambda$  and the photoelastic coefficient  $\rho_\alpha$  of the LCFBG. In our proposed system, a practical way to increase the sensitivity is to increase the dispersion value  $\ddot{\Phi}_\lambda$ . By increasing the dispersion value of the DCF in our system, the sensitivity would be improved. However, the temporal width of the stretched pulse will be increased by using a longer DCF. As a result, the width of the compressed pulse would also be increased, which would lead to a lower temporal resolution. Therefore, there is a tradeoff between the sensitivity and the resolution.

## V. CONCLUSION

We have proposed and experimentally demonstrated a novel approach to interrogating an LCFBG sensor based on SS-WTT mapping with both increased resolution and SNR. In the proposed system, an LCFBG was incorporated in one arm of an MZI, making the MZI have a spectral response with increasing or decreasing FSR. When the LCFBG was experiencing a strain, the strain information was conveyed to a wavelength shift, which was further transferred to the change of the FSR. If an ultra-short pulse was spectrum shaped by

the MZI, the shaped spectrum would contain the information of the wavelength shift. The demodulation was performed in the time domain by mapping the shaped spectrum to the temporal domain using a dispersive element. The generated temporal waveform was then correlated with a special reference waveform, with the location of the correlation peak indicating the wavelength shift of the LCFBG. The key significance of the proposed technique is that the generated waveform is compressed, thus the interrogation resolution is greatly improved. In addition, since an LCFBG has a broader bandwidth, the use of the LCFBG as a sensing element would make the output waveform have a broader temporal duration, which again leads to an increased SNR. The proposed approach has the advantages of real-time interrogation, high resolution and improved SNR, which can find applications where high-speed and high precision sensing is required.

## APPENDIX

In this Appendix, we develop (3), (9), and (15). The derivation of (3) is as follows:

$$\begin{aligned}
 H_2(\omega) &\cong \frac{1}{2} \left[ \exp\left(-j\omega t_1 + j\frac{\ddot{\Phi}_v}{2}\omega^2\right) + \exp(-j\omega t_2) \right] \\
 &= \frac{1}{2} \left[ \exp\left(j\frac{\ddot{\Phi}_v}{2}\omega^2\right) + \exp(-j\omega\Delta t) \right] \exp(-j\omega t_1) \\
 &= \cos\left(\frac{\frac{\ddot{\Phi}_v}{2}\omega^2 + \omega\Delta t}{2}\right) \\
 &\quad \times \exp\left(-j\omega t_1 + j\frac{\frac{\ddot{\Phi}_v}{2}\omega^2 - \omega\Delta t}{2}\right) \\
 &= \frac{\sqrt{2}}{2} \sqrt{1 + \cos\left(\frac{\ddot{\Phi}_v}{2}\omega^2 + \omega\Delta t\right)} \\
 &\quad \times \exp\left(-j\omega t_1 + j\frac{\frac{\ddot{\Phi}_v}{2}\omega^2 - \omega\Delta t}{2}\right). \tag{22}
 \end{aligned}$$

The derivation of (9) is given as

$$\begin{aligned}
 s_p(t) &= R|y(t)|^2 \\
 &\cong R \left| \exp\left(j\frac{1}{2\ddot{\Phi}}t^2\right) P_1(\omega) \Big|_{\omega=t/\ddot{\Phi}} \right|^2 \\
 &= \frac{RA_1^2}{8} \exp\left[-\left(\frac{\omega - \omega_{F0}}{B_F}\right)^2\right] \\
 &\quad \times \left[ 1 + \cos\left(\frac{\ddot{\Phi}_v}{2}\omega^2 + \omega\Delta t\right) \right] \Big|_{\omega=t/\ddot{\Phi}} \\
 &= \frac{RA_1^2}{8} \exp\left[-\left(\frac{\frac{2\pi c}{\lambda} - \omega_{F0}}{B_F}\right)^2\right] \\
 &\quad \times \left[ 1 + \cos\left(\frac{\ddot{\Phi}_v}{2}\omega^2 + \omega\Delta t\right) \right] \Big|_{\omega=t/\ddot{\Phi}} \tag{23}
 \end{aligned}$$

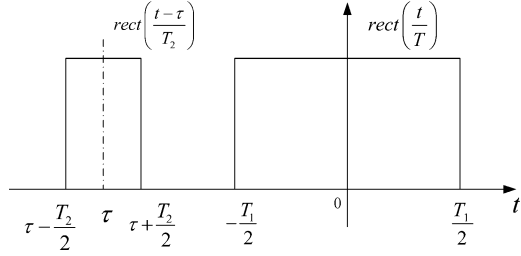


Fig. 4. The definition of the rectangular functions.

$$\begin{aligned}
 s_p(t) &= T(\lambda) \left[ 1 + \cos \left( \frac{\ddot{\Phi}_v}{2} \omega^2 + \omega \Delta t \right) \right] \Big|_{\omega=t/\ddot{\Phi}} \\
 &= T(\lambda) \left\{ 1 + \cos \left[ -\frac{\ddot{\Phi}_\lambda \lambda_0^2}{2\pi c} \left( \frac{2\pi c}{\lambda} \right)^2 + \frac{2\pi c}{\lambda} \Delta t \right] \right\} \Big|_{\lambda=t/\ddot{\Phi}_\lambda} \\
 &\cong T(\lambda) \left\{ 1 + \cos \left[ -\frac{2\pi n_{\text{eff}}}{\lambda_0^2} \frac{\lambda^2}{C} \right. \right. \\
 &\quad \left. \left. + \frac{2\pi n_{\text{eff}}}{\lambda_0^2} \left( \Delta L + 2\frac{\Delta\lambda}{C} \right) \lambda \right] \right\} \Big|_{\lambda=t/\ddot{\Phi}_\lambda} \\
 &= T \left( \frac{t}{\ddot{\Phi}_\lambda} \right) \left\{ 1 + \cos \left[ \frac{2\pi n_{\text{eff}}}{C \lambda_0^2 \ddot{\Phi}_\lambda^2} t(t + 2\Delta t_c(z)) \right. \right. \\
 &\quad \left. \left. + C \ddot{\Phi}_\lambda \Delta L \right] \right\} \quad (24)
 \end{aligned}$$

where

$$T(\lambda) = \frac{RA_1^2}{8} \exp \left[ - \left( \frac{\frac{2\pi c}{\lambda} - \omega_{F0}}{B_F} \right)^2 \right].$$

The derivation of the cross correlation of the two chirped microwave waveforms is as follows:

$$\begin{aligned}
 R_{T_1 T_2}(\tau) &= \frac{1}{2} s_{T_1}(-\tau)^* * s_{T_2}(\tau) \\
 &= \frac{1}{2} \int_{-\infty}^{+\infty} \text{rect} \left( \frac{-t}{T_1} \right) e^{j\pi \cdot k \cdot t^2} \text{rect} \left( \frac{\tau - t}{T_2} \right) \\
 &\quad \times e^{j\pi \cdot k \cdot (\tau - t)^2} e^{j\pi \cdot k \cdot \Delta t_c(z) \cdot (\tau - t)} dt \\
 &= \frac{1}{2} \cdot e^{j\pi \cdot k \cdot \tau [\tau + \Delta t_c(z)]} \\
 &\quad \times \int_{-\infty}^{+\infty} \\
 &\quad \times \text{rect} \left( \frac{-t}{T_1} \right) \text{rect} \left( \frac{\tau - t}{T_2} \right) e^{-j\pi \cdot k \cdot [2\tau + \Delta t_c(z)] \cdot t} dt. \quad (25)
 \end{aligned}$$

It is known that

$$\text{rect} \left( \frac{\tau - t}{T_1} \right) = \text{rect} \left( \frac{t - \tau}{T_1} \right). \quad (26)$$

Then, we define the corresponding limits for the intervals, as shown in Fig. 4.

For further calculation, we have to consider the corresponding cases of the overlapping rectangular function:

Case 1:

$$\tau + \frac{T_2}{2} < -\frac{T_1}{2} \Rightarrow \tau < -\frac{T_1 + T_2}{2} \quad (27)$$

$$R_{12}(\tau) = 0. \quad (28)$$

Case 2:

$$\begin{aligned}
 \tau - \frac{T_2}{2} < -\frac{T_1}{2} \leq \tau + \frac{T_2}{2} \Rightarrow \\
 -\frac{T_1 + T_2}{2} \leq \tau < -\frac{T_1 - T_2}{2} \quad (29)
 \end{aligned}$$

$$\begin{aligned}
 R_{T_1 T_2}(\tau) &= \frac{1}{2} e^{j\pi k \tau [\tau + \Delta t_c(z)]} \\
 &\quad \times \int_{-\infty}^{+\infty} \text{rect} \left( \frac{-t}{T_1} \right) \text{rect} \left( \frac{\tau - t}{T_2} \right) \\
 &\quad \times e^{-j\pi k [2\tau + \Delta t_c(z)] t} dt \\
 &= \frac{1}{2} e^{j\pi k \tau [\tau + \Delta t_c(z)]} \frac{e^{-j\pi k [2\tau + \Delta t_c(z)] t}}{-j2\pi k \left[ \tau + \frac{\Delta t_c(z)}{2} \right]} \Big|_{-\frac{T_1}{2}}^{\tau + \frac{T_2}{2}} \\
 &= \frac{1}{2} \left( \tau + \frac{T_1 + T_2}{2} \right) e^{-j\pi k \left\{ \left[ \tau + \frac{\Delta t_c(z)}{2} \right] \frac{T_1 - T_2}{2} + \frac{\Delta t_c(z) \tau}{2} \right\}} \\
 &\quad \times \text{sinc} \left\{ \pi k \left[ \tau + \frac{\Delta t_c(z)}{2} \right] \left( \tau + \frac{T_1 + T_2}{2} \right) \right\}. \quad (30)
 \end{aligned}$$

Case 3:

$$\tau + \frac{T_2}{2} < \frac{T_1}{2} \quad \text{and} \quad \tau - \frac{T_2}{2} \geq -\frac{T_1}{2} \quad (31a)$$

$$\Rightarrow -\frac{T_1 - T_2}{2} \leq \tau < \frac{T_1 - T_2}{2}. \quad (31b)$$

Thus

$$\begin{aligned}
 R_{T_1 T_2}(\tau) &= \frac{1}{2} e^{j\pi k \tau [\tau + \Delta t_c(z)]} \\
 &\quad \times \int_{-\infty}^{+\infty} \text{rect} \left( \frac{-t}{T_1} \right) \text{rect} \left( \frac{\tau - t}{T_2} \right) \\
 &\quad \times e^{-j\pi k [2\tau + \Delta t_c(z)] t} dt \\
 &= \frac{1}{2} e^{j\pi \cdot k \cdot \tau [\tau + \Delta t_c(z)]} \frac{e^{-j\pi k [2\tau + \Delta t_c(z)] t}}{-j2\pi k \left[ \tau + \frac{\Delta t_c(z)}{2} \right]} \Big|_{\tau - \frac{T_2}{2}}^{\tau + \frac{T_2}{2}} \\
 &= \frac{T_2}{2} e^{-j\pi \cdot k \cdot \tau^2} \text{sinc} \left( \pi k \left[ \tau + \frac{\Delta t_c(z)}{2} \right] T_2 \right). \quad (32)
 \end{aligned}$$

Case 4:

$$\tau - \frac{T_2}{2} < \frac{T_1}{2} \leq \tau + \frac{T_2}{2} \Rightarrow \frac{T_1 - T_2}{2} \leq \tau < \frac{T_1 + T_2}{2} \quad (33)$$

$$\begin{aligned}
R_{T_1 T_2}(\tau) &= \frac{1}{2} e^{j\pi k \tau [\tau + \Delta t_c(z)]} \\
&\times \int_{-\infty}^{+\infty} \text{rect}\left(\frac{-t}{T_1}\right) \text{rect}\left(\frac{\tau - t}{T_2}\right) \\
&\times e^{-j\pi k [2\tau + \Delta t_c(z)]t} dt \\
&= \frac{1}{2} e^{j\pi k \tau [\tau + \Delta t_c(z)]} \frac{e^{-j\pi k [2\tau + \Delta t_c(z)]t}}{-j2\pi k \left[\tau + \frac{\Delta t_c(z)}{2}\right]} \Bigg|_{\tau - \frac{T_2}{2}}^{\frac{T_1}{2}} \\
&= \frac{1}{2} \left(\frac{T_1 + T_2}{2} - \tau\right) e^{j\pi k \left\{ \left[\tau + \frac{\Delta t_c(z)}{2}\right] \frac{T_1 - T_2}{2} - \frac{\Delta t_c(z)\tau}{2} \right\}} \\
&\times \text{sinc}\left(\pi k \left[\tau + \frac{\Delta t_c(z)}{2}\right] \left(\tau - \frac{T_1 + T_2}{2}\right)\right). \quad (34)
\end{aligned}$$

Case 5:

$$\tau - \frac{T_2}{2} \geq \frac{T_1}{2} \Rightarrow \tau \geq \frac{T_1 + T_2}{2} \quad (35)$$

$$R_{12}(\tau) = 0. \quad (36)$$

Summary of cases 2, 3 and 4:

$$-\frac{T_1 + T_2}{2} \leq \tau < \frac{T_1 + T_2}{2}. \quad (37)$$

For Case 2, we have

$$\begin{aligned}
R_{T_1 T_2}(\tau) &= \frac{1}{2} \left(\tau + \frac{T_1 + T_2}{2}\right) \\
&\times e^{-j\pi k \left\{ \left[\tau + \frac{\Delta t_c(z)}{2}\right] \frac{T_1 - T_2}{2} + \frac{\Delta t_c(z)\tau}{2} \right\}} \\
&\times \text{sinc}\left\{\pi k \left[\tau + \frac{\Delta t_c(z)}{2}\right] \left(\tau + \frac{T_1 + T_2}{2}\right)\right\}. \quad (38)
\end{aligned}$$

For Case 3, we have

$$R_{T_1 T_2}(\tau) = \frac{T_2}{2} e^{-j\pi k \cdot \tau^2} \text{sinc}\left(\pi k \left[\tau + \frac{\Delta t_c(z)}{2}\right] T_2\right) \quad (39)$$

For Case 4, we have

$$\begin{aligned}
R_{T_1 T_2}(\tau) &= \frac{1}{2} \left(\frac{T_1 + T_2}{2} - \tau\right) \\
&\times e^{j\pi k \left\{ \left[\tau + \frac{\Delta t_c(z)}{2}\right] \frac{T_1 - T_2}{2} - \frac{\Delta t_c(z)\tau}{2} \right\}} \\
&\times \text{sinc}\left(\pi k \left[\tau + \frac{\Delta t_c(z)}{2}\right] \left(\tau - \frac{T_1 + T_2}{2}\right)\right). \quad (40)
\end{aligned}$$

Therefore, we have the correlation

$$\begin{aligned}
R_{12}(\tau) &= \text{Re}\{R_{T_1 T_2}(\tau) e^{j2\pi f_0 t}\} \\
&= \frac{1}{2} w(\tau) \text{sinc}\left\{\pi k \left[\tau + \frac{\Delta t_c(z)}{2}\right] w(\tau)\right\} \\
&\times \cos(2\pi f_e \tau + \varphi) \quad (41)
\end{aligned}$$

where  $w(\tau)$ ,  $f_e$  and  $\varphi$  are given by (17), (18), and (19) respectively.

## REFERENCES

- [1] K. P. Koo, A. B. Tveten, and S. T. Vohra, "Dense wavelength division multiplexing of fibre Bragg grating sensors using CDMA," *Electron. Lett.*, vol. 35, no. 2, pp. 165–167, Jan. 1999.
- [2] P. K. C. Chan, W. Jin, J. M. Gong, and M. S. Demokan, "Multiplexing of fiber Bragg grating sensors using an FMCW technique," *IEEE Photon. Technol. Lett.*, vol. 11, no. 11, pp. 1470–1472, Nov. 1999.
- [3] S. M. Melle, K. Liu, and R. M. Measures, "A passive wavelength demodulation system for guided-wave Bragg grating sensors," *IEEE Photon. Technol. Lett.*, vol. 4, no. 5, pp. 516–518, May 1992.
- [4] Q. Zhang, D. A. Brown, H. Kung, J. E. Townsend, M. Chen, L. J. Reinhart, and T. F. Morse, "Use of highly overcoupled couplers to detect shifts in Bragg wavelength," *Electron. Lett.*, vol. 31, no. 6, pp. 480–482, Mar. 1995.
- [5] H. Xia, C. Zhang, H. Mu, and D. Sun, "Edge technique for direct detection of strain and temperature based on optical time domain reflectometry," *Appl. Opt.*, vol. 48, no. 2, pp. 189–197, Jan. 2009.
- [6] A. D. Kersey, M. A. Davis, H. J. Patrick, M. LeBlanc, K. P. Koo, C. G. Askins, M. A. Putnam, and E. J. Friebele, "Fiber grating sensors," *J. Lightw. Technol.*, vol. 15, no. 8, pp. 1442–1463, Aug. 1997.
- [7] C. G. Askins, M. A. Putnam, G. M. Williams, and E. J. Friebele, "Stepped-wavelength optical fiber Bragg grating arrays fabricated in line on a draw tower," *Opt. Lett.*, vol. 19, no. 2, pp. 147–149, Jan. 1994.
- [8] R. Willsch, W. Ecke, and H. Bartelt, "Optical fiber grating sensor networks and their application in electric power facilities, aerospace and geotechnical engineering," in *15th Opt. Fiber Sensors Conf. Tech. Dig.*, Portland, OR, Aug. 7, 2002, Paper TuA1.
- [9] M. LeBlanc, S. Y. Huang, M. Ohn, R. M. Measures, A. Guemes, and A. Othonos, "Distributed strain measurement based on a fiber Bragg grating and its reflection spectrum analysis," *Opt. Lett.*, vol. 21, no. 17, pp. 1405–1407, Sep. 1996.
- [10] A. D. Kersey and T. A. Berkoff, "Fiber-optic Bragg grating differential-temperature sensor," *IEEE Photon. Technol. Lett.*, vol. 4, no. 10, pp. 1183–1285, Oct. 1992.
- [11] Y. J. Rao, D. A. Jackson, L. Zhang, and I. Bennion, "Dual-cavity interferometric wavelength-shift detection for in-fiber Bragg grating sensors," *Opt. Lett.*, vol. 21, no. 19, pp. 1556–1558, Oct. 1996.
- [12] B. Lee, Y. W. Lee, and J. Jung, "Applications of long-period fiber grating pair interferometers for sensors and communications," in *15th Annu. Meeting IEEE LEOS*, 2002, Paper TuE1.
- [13] H. Y. Xia, C. Wang, S. Blais, and J. P. Yao, "Ultrafast and precise interrogation of fiber Bragg grating sensor based on wavelength-to-time mapping incorporating higher order dispersion," *J. Lightw. Technol.*, vol. 28, no. 3, pp. 254–261, Feb. 2010.
- [14] T. Jansson, "Real-time Fourier transformation in dispersive optical fibers," *Opt. Lett.*, vol. 8, no. 4, pp. 232–234, Apr. 1983.
- [15] M. A. Muriel, J. Azana, and A. Carballar, "Real-time Fourier transformer based on fiber gratings," *Opt. Lett.*, vol. 24, no. 1, pp. 1–3, Jan. 1999.
- [16] J. Chou, D. R. Solli, and B. Jalali, "Real-time spectroscopy with subgigahertz resolution using amplified dispersive Fourier transformation," *Appl. Phys. Lett.*, vol. 92, no. 11, pp. 1111021–1111023, Mar. 2008.
- [17] K. Goda, K. K. Tsia, and B. Jalali, "Serial time-encoded amplified imaging for real-time observation of fast dynamic phenomena," *Nature*, vol. 458, pp. 1145–1150, Apr. 2009.
- [18] C. Wang and J. P. Yao, "Chirped microwave pulse generation based on optical spectral shaping and wavelength-to-time mapping using a sagnac loop mirror incorporating a chirped fiber Bragg grating," *J. Lightw. Technol.*, vol. 27, no. 16, pp. 3336–3341, Aug. 2009.
- [19] D. K. Barton, *Radar System Analysis and Modeling*. Boston, MA: Artech House, 2005.
- [20] J. Azaña and M. A. Muriel, "Real-time optical spectrum analysis based on the time-space duality in chirped fiber gratings," *IEEE J. Quantum Electron.*, vol. 36, no. 5, pp. 517–526, May 2000.
- [21] Y. J. Rao, "In-fibre Bragg grating sensors," *Meas. Sci. Technol.*, vol. 8, no. 4, pp. 355–375, Apr. 1997.

**Weilin Liu** (S'10) received the B.Eng. degree in electronic information engineering from the University of Science and Technology of China, Hefei, China, in 2009. He is currently working toward the M.A.Sc. degree in electrical and computer engineering at the School of Information Technology and Engineering, University of Ottawa, Ottawa, ON, Canada.

His research interests include optical signal processing, fiber Bragg grating and their applications in microwave photonics systems.

Mr. Liu is a student member of the IEEE Microwave Theory and Techniques Society.

**Ming Li** (S'08–M'09) received the Ph.D. degree in electrical and electronics engineering from the University of Shizuoka, Hamamatsu, Japan, in 2009.

In April 2009, he joined the Microwave Photonics Research Laboratory, School of Information Technology and Engineering, University of Ottawa, Ottawa, ON, Canada, as a Postdoctoral Research Fellow. His current research interests include advanced fiber Bragg grating and its applications to microwave photonics, ultrafast optical signal processing, arbitrary waveform generation and optical MEMS sensing.

**Chao Wang** (S'08) received the B.Eng. degree in opto-electrical engineering from Tianjin University, Tianjin, China, in 2002, and the M.Sc. degree in optics from Nankai University, Tianjin, China, in 2005. He is currently working toward the Ph.D. degree in electrical and computer engineering at the School of Information Technology and Engineering, University of Ottawa, Ottawa, ON, Canada.

His research interests include all-optical microwave waveform generation and processing, coherent optical pulse shaping, optical signal processing, radio-over-fiber systems, fiber Bragg gratings and their applications in microwave photonics systems.

Mr. Wang is a student member of the IEEE Photonics Society, the IEEE Microwave Theory and Techniques Society, the Optical Society of America, and the International Society for Optical Engineering.

**Jianping Yao** (M'99–SM'01) received the Ph.D. degree in electrical engineering from the Université de Toulon, Toulon, France, in 1997.

He joined the School of Information Technology and Engineering, University of Ottawa, ON, Canada, in 2001, where he is currently a Professor, Director of the Microwave Photonics Research Laboratory, and Director of the Ottawa-Carleton Institute for Electrical and Computer Engineering. From 1999 to 2001, he held a faculty position with the School of Electrical and Electronic Engineering, Nanyang Technological University, Singapore. He holds a Yongqian Endowed Visiting Chair Professorship with Zhejiang University, China. He spent three months as an invited professor in the Institut National Polytechnique de Grenoble, France, in 2005. His research has focused on microwave photonics, which includes all-optical microwave signal processing, photonic generation of microwave, mm-wave and THz, radio over fiber, UWB over fiber, fiber Bragg gratings for microwave photonics applications, and optically controlled phased array antenna. His research interests also include fiber lasers, fiber-optic sensors and bio-photonics. He is an associate editor of the *International Journal of Microwave and Optical Technology*. He has authored or coauthored over 300 papers, including over 170 papers in refereed journals and over 130 papers in conference proceeding.

Dr. Yao is a Registered Professional Engineer of the Province of Ontario. He is a Fellow of the Optical Society of America and a Senior Member of the IEEE Photonics Society and the IEEE Microwave Theory and Techniques Society. He is on the Editorial Board of the IEEE TRANSACTIONS ON MICROWAVE THEORY AND TECHNIQUES. He was the recipient of the 2005 International Creative Research Award of the University of Ottawa, the 2007 George S. Glinski Award for Excellence in Research, and an NSERC Discovery Accelerator Supplements award in 2008. He was named University Research Chair in Microwave Photonics in 2007.